Mathematical Biosciences and Engineering

MBE, 21(3): 3838–3859.
DOI: 10.3934/mbe.2024171
Received: 13 December 2023
Revised: 01 February 2024
Accepted: 02 February 2024
Published: 20 February 2024

https://www.aimspress.com/journal/MBE

Research article

Predicting the cognitive function status in end-stage renal disease patients at a functional subnetwork scale

Yu Lu[1,†], Tongqiang Liu[2,†], Quan Sheng[1], Yutao Zhang[1], Haifeng Shi[3,*] and Zhuqing Jiao[1,4,*]

[1] School of Microelectronics and Control Engineering, Changzhou University, Changzhou 213164, China
[2] Department of Nephrology, The Affiliated Changzhou No.2 People's Hospital of Nanjing Medical University, Changzhou 213003, China
[3] Department of Radiology, The Affiliated Changzhou No.2 People's Hospital of Nanjing Medical University, Changzhou 213003, China
[4] School of Computer Science and Artificial Intelligence, Changzhou University, Changzhou 213164, China

* **Correspondence**: Email: doctorstone771@163.com, jzq@cczu.edu.cn.

† The authors contributed equally to this work.

Abstract: Brain functional networks derived from functional magnetic resonance imaging (fMRI) provide a promising approach to understanding cognitive processes and predicting cognitive abilities. The topological attribute parameters of global networks are taken as the features from the overall perspective. It is constrained to comprehend the subtleties and variances of brain functional networks, which fell short of thoroughly examining the complex relationships and information transfer mechanisms among various regions. To address this issue, we proposed a framework to predict the cognitive function status in the patients with end-stage renal disease (ESRD) at a functional subnetwork scale (CFSFSS). The nodes from different network indicators were combined to form the functional subnetworks. The area under the curve (AUC) of the topological attribute parameters of functional subnetworks were extracted as features, which were selected by the minimal Redundancy Maximum Relevance (mRMR). The parameter combination with improved fitness was searched by the enhanced whale optimization algorithm (E-WOA), so as to optimize the parameters of support vector regression (SVR) and solve the global optimization problem of the predictive model. Experimental results indicated that CFSFSS achieved superior predictive performance compared to other methods, by which the mean absolute error (MAE), mean absolute percentage error (MAPE), and root mean square error (RMSE) were up to 0.5951, 0.0281 and 0.9994, respectively. The functional

subnetwork effectively identified the active brain regions associated with the cognitive function status, which offered more precise features. It not only helps to more accurately predict the cognitive function status, but also provides more references for clinical decision-making and intervention of cognitive impairment in ESRD patients.

Keywords: cognitive function status; functional subnetwork; enhanced whale optimization algorithm; support vector regression; prediction

Abbreviations: fMRI: functional magnetic resonance imaging; ESRD: end-stage renal disease; CFSFSS: the cognitive function status at functional subnetwork scale; AUC: area under the curve; mRMR: minimal Redundancy Maximum Relevance; E-WOA: enhanced whale optimization algorithm; SVR: support vector regression; MAE: mean absolute error; MAPE: mean absolute percentage error; RMSE: root mean square error; NC: normal control; MoCA: Montreal Cognitive Assessment; AAL: Automated Anatomical Labeling; WOA: whale optimization algorithm; LOO-CV: leave-one-out cross-validation

1. Introduction

End-stage renal disease (ESRD) is a severe kidney disorder that significantly impairs kidney function, resulting in an inability to meet the body's metabolic and waste excretion requirements. Approximately 50,000 ESRD patients die annually in the United States [1]. In addition to its impact on physical function, ESRD can have detrimental effects on cognitive function. Cognitive impairment is commonly observed in ESRD patients, with studies reporting that 30 to 70% of individuals with ESRD experience varying degrees of cognitive impairment [2]. This impairment can manifest as memory loss, lack of concentration, executive dysfunction, and other symptoms, significantly affecting their quality of life and daily functioning.

Cognitive impairment can lead to challenges in medication management, medical decision-making, and treatment adherence among ESRD patients, thereby increasing their healthcare risks [3]. Importantly, cognitive impairment can also impact driving ability, work capacity, and social interactions, posing limitations on the independence and participation of individuals with ESRD in their daily lives [4]. It is crucial to detect cognitive impairment early and implement appropriate interventions for reducing symptoms and enhancing the quality of life for ESRD patients. However, the current diagnosis of cognitive function status primarily relies on scoring measures from assessment scales, which have certain drawbacks.

Clinicians spend considerable time recording patients' feedback using these scales, and the experience level of the clinician can significantly influence the scores of cognitive function status assessments [5]. Moreover, different biological causes can manifest as the same behavioral phenotype, making diagnosis more challenging [6]. In recent years, advancements in imaging technology and the application of complex network analysis in neuroscience research have provided new perspectives for diagnosing cognitive status [7]. The brain is a complex organ with billions of neurons forming intricate connectivity networks through synapses. The connections between different brain regions can influence cognitive function status [8]. Therefore, studying cognitive function status from the perspective of brain functional networks offers a novel approach to diagnosis.

We aimed to address the limitations of traditional assessment scales in accurately measuring the cognitive function status of ESRD patients with cognitive impairment. In light of this, a method based on functional subnetwork is proposed to predict the cognitive function status (CFSFSS) of ESRD patients. Unlike previous approaches, we focus on capturing the relationship between nodes and cognitive functional status from the perspective of functional subnetworks. In this study, introduce several key contributions and novel aspects: (a) Subnetwork Construction: Nodes from diverse network indicators are carefully selected, and their connectivity is extracted to construct functional subnetworks. This approach allows us to capture the intricate relationships between nodes and the cognitive functional status of ESRD patients. (b) Enhanced Optimization Algorithm: We employ the enhanced Whale Optimization Algorithm (E-WOA) to optimize the parameters of SVR. This algorithmic approach ensures more accurate parameter optimization, contributing to improved predictive performance. (c) Addressing Limitations: We aimed to overcome the limitations of traditional assessment scales in accurately measuring the cognitive function status of ESRD patients with cognitive impairment. By focusing on functional subnetworks and their connections, we gain a deeper understanding of the important links between cognitive processes and nodes within the networks.

The rest of this work is organized as follows: Section 2 gives the literature review of the work. Section 3 provides the materials and methods. Section 4 introduces the results of the related work. Sections 5 and 6 present the discussions and conclusions, respectively.

2. Literature review

2.1. Related studies

Numerous studies have investigated the potential of using brain functional networks to understand cognitive processes and predict cognitive function status. Li et al. [9] constructed two brain network models to evaluate the cognitive function in patients with amnestic mild cognitive impairment (aMCI). Zhou et al. [10] proposed a method to assess the structural basis of the functional connectivity (FC) alterations in Alzheimer's disease (AD) by investigating the relationship between FC and structural connectivity (SC) in the default mode network (DMN). Zhang et al. [11] used graph theory to analyze the changes of functional brain networks among patients on maintenance hemodialysis (MHD) with and without cognitive impairment (CI).

Researchers have also made contributions to explore various approaches for analyzing brain disorders and investigate cognitive impairment in specific conditions. Zhang et al. [12] selected multiple node statistics jointly from brain functional networks for identifying brain disorders. Min et al. [13] computed degree centrality (DC) to investigate the intrinsic dysconnectivity pattern of the brain in post stroke cognitive impairment (PSCI) patients. Both methods provided valuable insights into the underlying neural mechanisms of cognitive processes and their implications.

Previous studies have employed various optimization techniques to enhance the predictive performance of support vector regression (SVR) [14]. Mao et al. [15] considered that grid search plays a part in exploring the parameter space and finding the optimal parameter combination. Zeng et al. [16] proposed a laser ultrasonic detection method using support vector machine based on particle swarm optimization (PSO-SVM) algorithm.

2.2. Research methods

In this study, we propose a framework for predicting the cognitive function status at the functional subnetwork scale. Functional subnetworks are created by combining nodes from multiple network indicators, allowing for a more comprehensive representation of the complexities and variabilities of brain functional networks. The framework collects topological attribute parameters of functional subnetworks and utilizes the AUC as features. Feature selection is performed by the mRMR. To improve the SVR, the E-WOA is employed to search for optimal parameter combination. This optimization procedure is crucial in addressing the global optimization problem associated with the prediction.

2.3. Research gap

Previous research in the field has primarily focused on analyzing cognitive function status using global brain functional networks. Alternatively, individual variations in brain structure and function can introduce inaccuracies in interpreting cognitive function status solely based on global networks [17]. While these methods have provided valuable insights into the neural mechanisms underlying cognitive processes, challenges remain in improving the accuracy and reliability of predictions. One limitation of existing approaches is their tendency to converge on local optimal solutions, hindering the identification of the global optimal solution. Some algorithms also suffer from high computational costs or limited exploration of the search space, limiting their effectiveness.

In contrast, the proposed framework addresses these limitations. By focusing on functional subnetworks, it considers the individual nuances and variabilities of brain functional networks, leading to more precise predictions of cognitive function status. The advanced optimization algorithms, including the E-WOA, improve the search for optimal parameter combination in the SVR, mitigating the issue of converging on local optimal solutions. This significantly enhances the accuracy and reliability of the prediction. Table 1 shows the literature review.

Table 1. Literature review.

Years	Authors	Conclusions	Limitations
2021	D. Zhang, Y. Y. Chen, et al.	Using graph theory to analyze the changes of functional brain networks in patients on MHD with and without cognitive impairment.	These approaches mainly involve whole-brain functional networks, and there is a lack of studies on the modularity of interindividual brain networks.
2021	X. Li, C. J. Yang, et al.	Constructing two brain network models to evaluate the cognitive function in patients with aMCI.	
2022	B. Zhou, X. J. Dou, et al.	Abnormal parts of structural and functional connectivity were found under the default mode network in patients.	
2022	Y. Y. Zhang, Y. F. Xue, et al.	Selecting multiple node statistics jointly from brain functional networks for identifying brain disorders.	There are challenges in improving the accuracy and reliability of the prediction of cognitive functional status.
2023	Y. Min, C. Liu, et al.	Computing the DC to investigate the intrinsic dysconnectivity pattern of the brain in PSCI patients.	

3. Materials and methods

In this section, we detail the methods employed in the research. We began with a well-defined framework, then collected important data, extracted features from subnetworks, chose the most significant features, and then optimized the parameters of SVR using the E-WOA. Every stage was essential to our investigation.

3.1. Research framework

Figure 1 shows the overall research framework of CFSFSS, consisting of the following steps: (a) Preprocessing raw resting-state functional magnetic resonance imaging (fMRI) images; (b) acquiring time series for all brain regions; (c) constructing brain functional networks with time series; (d) forming functional subnetworks by extraction of the nodes from different network indicators; (e) extracting topological attribute parameters of the functional subnetworks as features; (f) selecting the two most discriminative features by the maximum Relevance Minimum Redundancy (mRMR); (g) optimizing the parameters of the SVR by the E-WOA; and (h) predicting cognitive function status scores for ESRD patients with cognitive impairment.

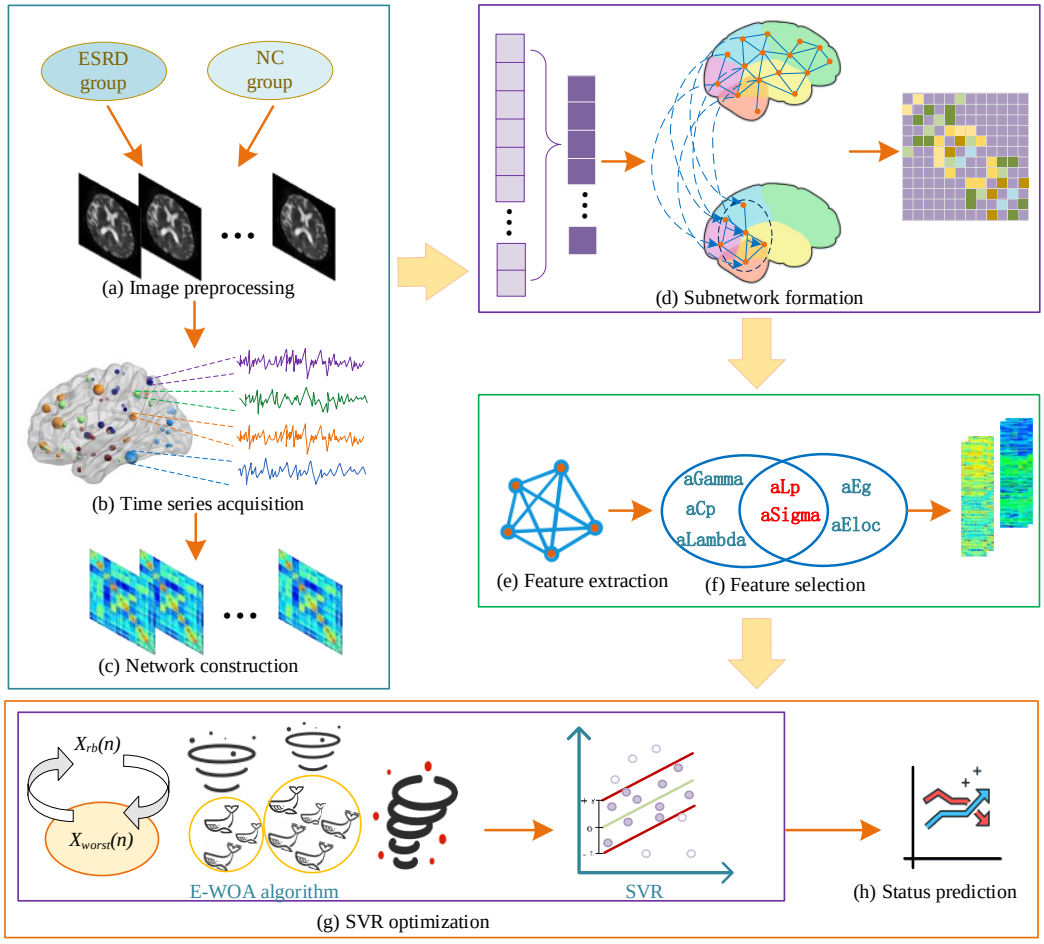

Figure 1. Research framework of CFSFSS.

3.2. Data collection

A total of 44 ESRD patients with cognitive impairment were admitted to the Affiliated Changzhou Second People's Hospital of Nanjing Medical University from May 2021 to March 2022. These patients are included in the ESRD group. Among them, there are 20 males and 24 females, with an age range of 34 to 66 years and a mean age of (50.05 ± 7.95) years. In addition, 30 healthy individuals who underwent physical examinations at the hospital during the same period are selected as the normal control (NC) group. The NC group consists of 19 males and 11 females, with an age range of 34 to 63 years and a mean age of (48.37 ± 6.70) years. There are no statistically significant differences in gender distribution, age, or education level between the ESRD group and the NC group ($P > 0.05$). All participants are right-handed and have no history of cardiovascular or cerebrovascular diseases, neurological disorders, infectious diseases, or diabetes. There are no contraindications for magnetic resonance imaging (MRI) examinations. Prior to fMRI acquisition, trained physicians assessed the subjects' cognitive function status according to the Montreal Cognitive Assessment (MoCA) scores. This study is conducted in accordance with the principles outlined in the Helsinki Declaration, and is approved by the Ethics Review Committee of the hospital. Table 2 shows the demographic information of the two groups of subjects.

Table 2. Demographic information.

	Gender (male/female)	Age (years, $\bar{x} \pm s$)	Education years(years, $\bar{x} \pm s$)	MoCA scores (points, $\bar{x} \pm s$)
ESRD group	20/24	50.05 ± 7.95	11.25 ± 3.19	21.36 ± 2.42
NC group	19/11	48.37 ± 6.70	9.73 ± 3.91	27.27 ± 1.26
p	0.134	0.346	0.071	***

Data collection is completed by the GE Discovery MR 750 W 3.0 T superconducting MR scanner equipped with a 32-channel head-neck coil. During the scanning process, the subject's head is fixed with a rubber soft match to avoid artifacts generated by head movement. Since then, the subjects should maintain a static and awake state to avoid thinking activities as much as feasible. Gradient Echo Planar Echo Imaging (GRE-EPI) sequence acquisition fMRI images. The machine scanning parameters are as follows: repetition time (TR) = 2000 ms, echo time (TE) = 40 ms, field of view (FOV) = 24 cm, flip angle (FA) = 90 degrees, matrix size = 64 × 64, and slice thickness = 6 mm.

The raw data are preprocessed with Data Processing Assistant for Resting-State fMRI (DPARSF) on the Matlab platform [18,19]. The specific steps are as follows: (a) Data format conversion: convert the original fMRI scan data from DICOM format to NIfTI format; (b) time point deletion: remove the initial time points accounting for subjects not being in a steady state; (c) slice timing correction: adjust the data from all slices to the same time point to eliminate the influence of temporal differences, as fMRI scans are conducted slice by slice; (d) head motion correction: correct the subject's head position to eliminate the effects of head motion during the scanning process; (e) data format normalization: transform the data to the standard Montreal Neurological Institute (MNI) template space to improve comparability across different individuals or studies; (f) data smoothing procession: smooth the data using a convolution Gaussian kernel to boost the signal-to-noise ratio and statistical efficiency; (g) date trends removal: remove linear or non-linear trends in data to eliminate the effects of device drift or other long-term changes during scanning; (h) band-pass filtering: retain a specific frequency range

of 0.01–0.08 Hz to eliminate high-frequency noise and low-frequency physiological fluctuations; and (i) time series extraction: divide the brain of each subject into 90 brain regions with the standard segmentation template Automated Anatomical Labeling (AAL), and extract the time series for each brain region.

3.3. Subnetwork-based feature extraction

Functional subnetwork scale can effectively reduce the dimensionality of the data, making predictive models easier to process and understand [20]. The brain functional networks are constructed by the correlation coefficients between the time series of each brain region [21]. Then, the value of each node in the brain functional networks is calculated by the Brain Connectivity Toolbox (BCT) [22]. We consider nodes ranking in the top 20% for node degree, local clustering coefficient, node betweenness centrality, and global efficiency to define functional subnetworks. It ensures a focused set of nodes that has been validated in previous studies [23].

As shown in Figure 2, functional subnetworks are formed by nodes that satisfy the aforementioned criteria. Next, the AUC of the attribute property parameters for each subnetwork are extracted with the graph theoretical network analysis toolbox (GRETNA), resulting in the feature space *S*. Among these features are network clustering coefficient (aCp), network gamma (aGamma), network lambda (aLambda), shortest path length (aLp), network sigma (aSigma), network global efficiency (aEg), and network local efficiency (aEloc).

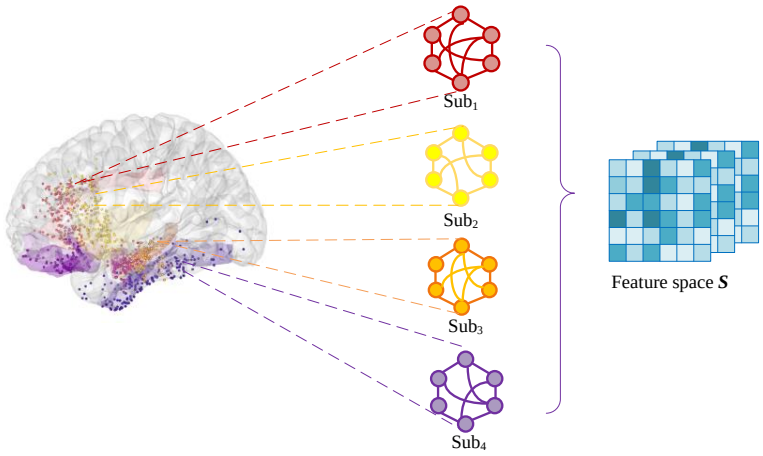

Figure 2. Construct the subnetworks and extract the feature.

3.4. Feature selection

The most informative features are identified by mRMR depending on the calculated metrics during the feature selection phase [24]. The dimensionality of the feature space is reduced to guarantee the accuracy and generalization capability of the predictive models. It facilitates the reduction of computational costs associated with data training and prediction [25]. Additionally, high-correlation feature selection can contribute to the interpretation of prediction results [26]. The mRMR is an information-theoretic feature selection method with an objective to identify a set of *m* features from the feature space *S* for each subnetwork. These selected features should exhibit high relevance to the

target class while minimizing redundancy among themselves. This selection process is guided by the maximum statistical dependency criterion, ensuring that the chosen features possessed maximum information content and are highly informative for the classification task. The definitions of maximum relevance and minimum redundancy are as follows:

Maximum relevance:

$$\max_{rele}(\boldsymbol{S},o)=\frac{1}{|\boldsymbol{S}|}\sum_{\boldsymbol{z}_u\in\boldsymbol{S}}\boldsymbol{I}(\boldsymbol{z}_u;o). \tag{1}$$

Minimum redundancy:

$$\min_{redu}(\boldsymbol{S})=\frac{1}{|\boldsymbol{S}|^2}\sum_{\boldsymbol{z}_u,\boldsymbol{z}_v\in\boldsymbol{S}}\boldsymbol{I}(\boldsymbol{z}_u;\boldsymbol{z}_v), \tag{2}$$

where $\boldsymbol{S}$ is the set of features; o is the target category; $\boldsymbol{I}(\boldsymbol{z}_u;o)$ is the mutual information between feature u and target category o; $\boldsymbol{I}(\boldsymbol{z}_u;\boldsymbol{z}_v)$ is the mutual information between feature u and feature v.

3.5. E-WOA-based SVR parameter optimization

The whale optimization algorithm (WOA) is a metaheuristic optimization technique that has demonstrated strong performance in a range of optimization problems. It is based on the hunting behavior of humpback whales. First, the WOA can efficiently search the parameter space and identify the optimal or nearly optimal solution due to its high exploration-utilization balance. This skill is essential for the intricate interaction that exists between the cognitive functional status of ESRD patients and features that are taken from functional subnetworks. Furthermore, the WOA has demonstrated its efficacy in addressing high-dimensional nonlinear optimization issues. Our research focuses on picking pertinent features and extracting features from functional subnetworks. The capacity of WOA to handle complicated, high-dimensional data makes it a perfect fit. It has some scalability and has been successfully used in a variety of domains, such as feature selection tasks and biomedical research. The algorithm's performance and optimization abilities can be enhanced by expanding the number of populations and incorporating novel behaviors. We can use this to further refine the algorithm.

The E-WOA is a variant of the original WOA [27]. It incorporates a shared pool mechanism [28] to store the worst search agents and generate new search agents through migration strategies, enhancing the algorithm's exploration capability. The fitness evaluation of each search agent is performed, and the best search agent is selected as the leader to guide the search process. Multiple search strategies, such as surrounding prey search, priority selection search, and spiral bubble-net attack, are employed to generate new search agents, thereby increasing the search diversity [29]. The inspiration for the E-WOA comes from the feeding behavior of whales, where they create bubble nets to trap prey while diving in a spiral path close to the water surface. Hunting behavior is divided into three stages: Encircling, bubble-net attack, and searching for prey.

The objective function is defined by specific parameter settings to evaluate SVR performance. A

set of search agents representing the SVR parameter set is randomly generated or initialized, and the search agent with the best fitness is selected as the leader.

Rounding up: The exact location of the prey is unknown in the encircling phase. Once whales detect signs of prey in their surroundings, they initiate an encircling behavior. Assuming the current best search agent is in proximity to the prey, other search agents adjust their positions to align with the best search agent. The mathematical expression for this behavior can be described as follows:

$$\boldsymbol{X}\left(n+1\right)=\boldsymbol{X}^{*}(n)-\boldsymbol{AT}\,, \tag{3}$$

$$\boldsymbol{T}=\left|\boldsymbol{CX}^{*}\left(n\right)-\boldsymbol{X}\left(n\right)\right|, \tag{4}$$

where n is the current number of iterations; $\boldsymbol{X}^{*}(n)$ is the best position vector obtained so far; $\boldsymbol{X}\left(n\right)$ is the current position vector; $\boldsymbol{A}$ and $\boldsymbol{C}$ are the coefficient vectors.

Bubble-net attack: Whales include two strategies during the prey attack phase, shrinking the encircling circle and spiral updating mechanism. The selection between bubble-net attack and shrinking the encircling circle is determined by the predation probability p. A logarithmic spiral equation serves to explain the position update between the whales and their prey:

$$\boldsymbol{X}(n+1)=\begin{cases}\boldsymbol{X}^{*}(n)-\boldsymbol{AT}, & p<0.5\\ \boldsymbol{T}^{'}e^{gl}\cdot\cos\left(2\pi l\right)+\boldsymbol{X}^{*}(n), & 0.5\le p<1\end{cases}, \tag{5}$$

$$\boldsymbol{T}^{'}=\left|\boldsymbol{X}^{*}\left(n\right)-\boldsymbol{X}\left(n\right)\right|, \tag{6}$$

where g is a constant and l is a random number between zero to one; $\boldsymbol{X}^{*}\left(n\right)$ is the best location for search agents; As the number of iterations increases, the coefficient vector $\boldsymbol{A}$ gradually decreases, and if $\left|\boldsymbol{A}\right|$ is less than one, then the bounding circle gradually tends to the optimal solution.

Searching for prey: The WOA adjusts the locations of the search agents, ensuring thorough examination of all whales during the encircling phase, by utilizing randomly selected ones. This randomization aims to enhance global search capability, prevent being trapped in local optima [30]. The mathematical expression for this process is as follows:

$$\boldsymbol{X}(n+1)=\boldsymbol{X}_{rand}(n)-\boldsymbol{AT}\,, \tag{7}$$

$$\boldsymbol{T}=\left|\boldsymbol{CX}_{rand}(n)-\boldsymbol{X}\left(n\right)\right|, \tag{8}$$

where $\boldsymbol{X}_{rand}(n)$ is the location of the search agent randomly selected from the current iteration.

The WOA has some shortcomings even if it exhibits good global search performance and quick convergence time, efficiently avoiding local optima. WOA has strong randomness when updating the whale position, which is easy to lead to premature convergence of the algorithm, and there are problems such as low population diversity and unbalanced search strategy [31].

Based on the WOA, E-WOA incorporates several enhancements to improve its performance. The primary one is the introduction of a pooling mechanism to store and release the positions of search agents [32]. The worst search agent location was mixed with the current search agent location to increase diversity. It helps to prevent the algorithm from falling into local optimality and improve its ability to explore the search space. The mathematical expression for this mechanism is as follows:

$$\boldsymbol{G}(n) = \boldsymbol{B}(n)\boldsymbol{X}_{rb}(n) + \overline{\boldsymbol{B}}(n)\boldsymbol{X}_{worst}(n), \tag{9}$$

where $\boldsymbol{B}(n)$ is a binary random vector and $\overline{\boldsymbol{B}}(n)$ is its inverse; $\boldsymbol{X}_{rb}(n)$ is a randomly generated location near the best search agent in the current iteration; $\boldsymbol{X}_{worst}(n)$ is the worst position of the search agent in the current iteration.

Migration search strategy: It entails randomly separating the whale population with an equation, which enhances population variety. Each separated subpopulation covers unexplored areas, reducing the occurrence of getting stuck in local optima. The mathematical expression for this strategy is as follows:

$$\boldsymbol{X}(n+1) = \boldsymbol{X}_{equal}(n) - \boldsymbol{X}_{rb}(n), \tag{10}$$

$$\boldsymbol{X}_{equal}(n) = l \cdot (\beta_{\max} - \beta_{\min}) + \beta_{\min}, \tag{11}$$

where $\boldsymbol{X}_{equal}(n)$ is a random location within the search space calculated by the equation; l is a random number between zero to one; $\beta_{\max}$ and $\beta_{\min}$ are the upper and lower bounds of the problem.

The other one is the incorporation of a priority selection search strategy, where the position of a search agent is updated by selecting the one with the highest fitness value. This aids in the convergence of search agents towards the best position. The mathematical expression for this strategy is as follows:

$$\boldsymbol{X}(n+1) = \boldsymbol{X}(n) + \boldsymbol{A}(\boldsymbol{C}g_{r1} - g_{r2}), \tag{12}$$

where g_{r1} and g_{r2} are random numbers selected from the pooling mechanism; $\boldsymbol{A}$ and $\boldsymbol{C}$ are vectors of coefficients.

The E-WOA incorporates a spiral bubble-net attack strategy, in which search agents move along a spiral path to converge towards the best position. This strategy helps improve the exploration of the search space and its ability to find the global optimum. The mathematical expression for this strategy is as follows:

$$\boldsymbol{X}(n+1) = \boldsymbol{X}^{*}(n) - \boldsymbol{A}\boldsymbol{T}', \tag{13}$$

$$\boldsymbol{T}' = \left|\boldsymbol{C}\boldsymbol{X}^{*}(n) - g_{r3}\right|, \tag{14}$$

where $\boldsymbol{X}^{*}(n)$ is the best location for search agents; g_{r3} is a random number selected from the

pooling mechanism.

According to the formulated strategy, the algorithm iteratively searches for the optimal combination of SVR parameters by adjusting the location of the search agent and evaluating its fitness. Through iterative execution of the above steps, the E-WOA is capable of searching for parameter combination with improved fitness to optimize the parameters of the SVR. After a certain number of iterations, the search agent with the best fitness can be selected as the optimal parameter combination for the E-WOA-optimized SVR.

4. Results

In this section, we present the experimental design, results, ablation study, and active brain regions analysis to validate the effectiveness of our framework.

4.1. Experimental design

The computed metrics are sorted in descending order to record the respective node IDs. Then, the nodes represented by the top 20% node IDs for each metric are extracted to generate four symmetric matrices, which are named "$Sub_1, Sub_2, Sub_3, Sub_4$" as the four functional subnetworks.

The functional subnetwork is sparsified by setting the threshold [33]. These thresholds are set in five ranges with a 0.01 step size: 0.1–0.6, 0.2–0.7, 0.3–0.8, 0.4–0.9, and 0.5–1.0. The AUC for small-world features and the overall effectiveness of all individuals are extracted with GRETNA [34]. Among these features are network clustering coefficient (aCp), network gamma (aGamma), network lambda (aLambda), shortest path length (aLp), network sigma (aSigma), network global efficiency (aEg), and network local efficiency (aEloc). The AUC of the two sets of topological attribute parameters differ considerably in the range of 0.2–0.7 across all matrix sparsity threshold ranges, so the matrix sparsity is set in this range.

Table 3 shows the results of feature selection with mRMR. The features aLp and aSigma are eliminated in Sub_1, Sub_2, and Sub_3, while the features aLp and aGamma are filtered out in Sub_4. To maintain the feature consistency, the number of features for Sub_4 is increased to three, revealing aSigma as the third feature. As a result, aLp and aSigma are selected as input variables for subsequent prediction analysis, ensuring the comparability and consistency of features.

Due to the limited sample size, the leave-one-out cross-validation (LOO-CV) strategy is applied to train different predictive models and evaluate the prediction accuracy [35]. Specifically, in each round of verification, a sample is first eliminated as a test set, and the leftovers are turned into a training set for regression prediction. To begin, the aLp and aSigma values of the ESRD group, along with the MoCA scores of the patients, have been combined into a single dataset. Following that, the dataset is divided into forty-four smaller subsets, with forty-three serving as training sets and one serving as the test set. This procedure is performed on all subsets to ensure that each data point is only for either training or testing, effectively removing data selection randomness. The mean absolute error (MAE), mean absolute percentage error (MAPE), and root mean square error (RMSE) are selected as the metrics for evaluating the prediction accuracy [36]. Lower MAE, MAPE, and RMSE values indicate higher prediction accuracy.

Table 3. Feature selection results in functional subnetworks.

Subnetwork	Feature	ESRD group(n = 44)	NC group(n = 30)	Feature selection results
Sub_1	aCp	0.123 ± 0.027	0.122 ± 0.025	
	aGamma	0.605 ± 0.070	0.615 ± 0.068	
	aLambda	0.535 ± 0.020	0.544 ± 0.020	
	aLp	1.561 ± 0.320	1.574 ± 0.269	√
	aSigma	0.564 ± 0.063	0.564 ± 0.060	√
	aEg	0.169 ± 0.039	0.165 ± 0.027	
	aEloc	0.195 ± 0.065	0.192 ± 0.045	
Sub_2	aCp	0.123 ± 0.027	0.122 ± 0.025	
	aGamma	0.604 ± 0.069	0.615 ± 0.069	
	aLambda	0.535 ± 0.020	0.544 ± 0.020	
	aLp	1.561 ± 0.320	1.574 ± 0.269	√
	aSigma	0.564 ± 0.062	0.564 ± 0.060	√
	aEg	0.169 ± 0.039	0.165 ± 0.027	
	aEloc	0.195 ± 0.065	0.192 ± 0.045	
Sub_3	aCp	0.106 ± 0.022	0.097 ± 0.019	
	aGamma	0.595 ± 0.063	0.602 ± 0.051	
	aLambda	0.533 ± 0.016	0.533 ± 0.014	
	aLp	1.602 ± 0.234	1.631 ± 0.288	√
	aSigma	0.557 ± 0.056	0.565 ± 0.047	√
	aEg	0.161 ± 0.027	0.159 ± 0.026	
	aEloc	0.186 ± 0.054	0.178 ± 0.043	
Sub_4	aCp	0.123 ± 0.025	0.121 ± 0.024	
	aGamma	0.611 ± 0.068	0.613 ± 0.074	√
	aLambda	0.537 ± 0.024	0.546 ± 0.025	
	aLp	1.561 ± 0.304	1.587 ± 0.253	√
	aSigma	0.568 ± 0.062	0.560 ± 0.061	
	aEg	0.168 ± 0.035	0.163 ± 0.024	
	aEloc	0.193 ± 0.061	0.193 ± 0.043	

4.2. Experimental results

The prediction results at the functional subnetwork scale and global network scale are compared by LOO-CV. Figure 3 shows prediction accuracy for different network modes, where the blue lines representing the real scores and the red lines representing the predicted scores. It indicates that the predictability at the functional subnetwork scale has improved to a certain extent compared to the global network. The overall predicted trends of real and predicted scores at the functional subnetwork scale are closer together than those at the global network scale. Additionally, Sub_3 produces closely matched predicted scores with little mistakes, indicating a closer match to the real scores.

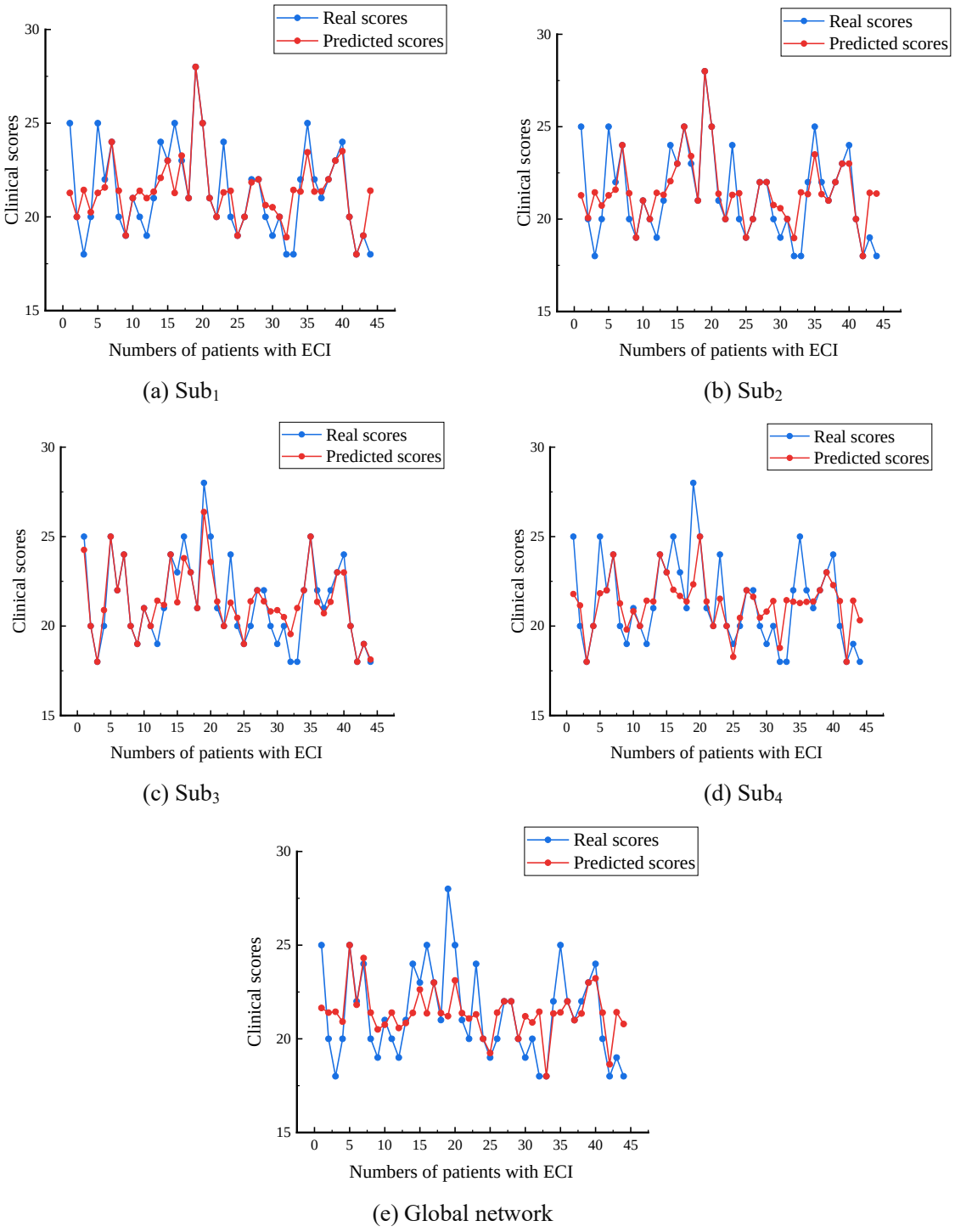

Figure 3. Prediction accuracy for different network modes.

Table 4 shows the prediction error values for various network modes. It is clear that Sub_3 produces superior prediction results. In terms of prediction accuracy, the functional subnetwork scale clearly outperforms the global network scale. Among them, it demonstrates considerable gains in the metrics of MAE, MAPE and RMSE. For example, the MAE, MAPE, and RMSE of clinical scores at Sub_3 are reduced by 0.695, 0.0317 and 0.9261, respectively, compared to the global network. This further confirms the superiority of CFSFSS, which can provide more exact prediction findings, thus improving

predict accuracy and efficiency.

Table 4. Prediction error values.

Network mode	MAE	MAPE	RMSE
Sub_1	0.9192	0.0435	1.5453
Sub_2	0.8953	0.0432	1.4971
Sub_3	0.5951	0.0281	0.9994
Sub_4	1.1002	0.0503	1.7101
Global network	1.2901	0.0598	1.9255

Inputting selected features into the E-WOA-optimized SVR can learn the correlation between features with stronger recognition. It is more conducive to explore the association between cognitive function status and scores, and improve the accuracy of score prediction. The prediction error values are shown in Figure 4, which were obtained with the WOA-optimized SVR and the E-WOA-optimized SVR for data prediction in Sub_3. The E-WOA-optimized SVR predicted MAE, MAPE, and RMSE of clinical scores at Sub_3, which are 0.2202, 0.0096, 0.5206 lower than those predicted by the WOA-optimized SVR, respectively. It shows that the E-WOA-optimized SVR can significantly improve the performance of score prediction compared with the WOA-optimized SVR.

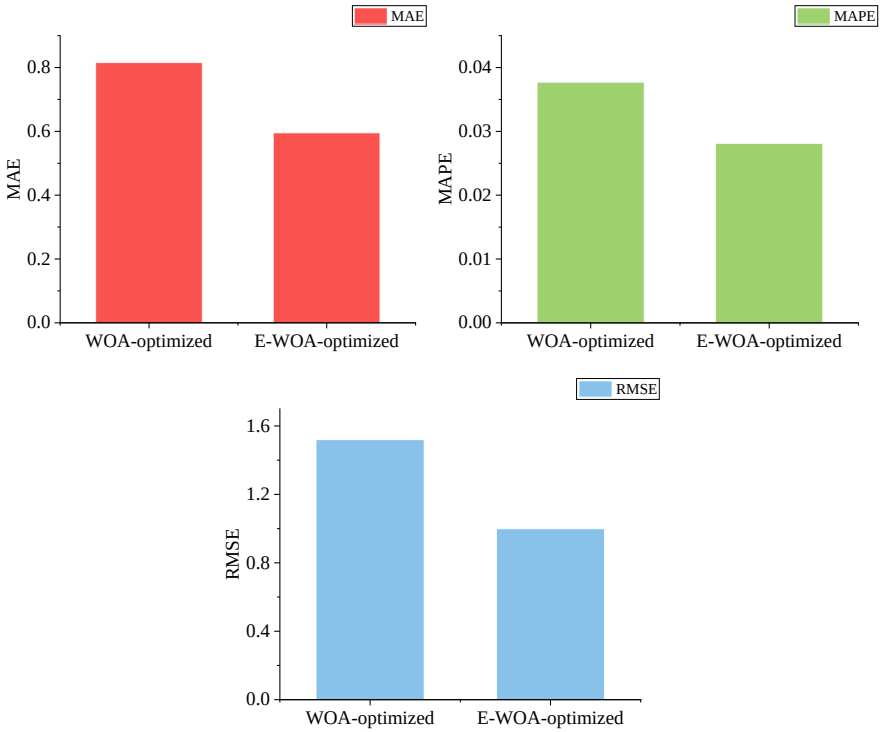

Figure 4. Prediction error values of the two optimization algorithms in Sub_3.

SVR is a popular and well-respected machine learning algorithm that has been effectively employed for a number of prediction applications, including the prediction of cognitive performance. When compared to other regression methods, SVR has the benefit of being less prone to overfitting and capable of handling non-linear connections between variables. Small sample problems can also be handled with the SVR algorithm. Given the relatively small sample size of the available medical data,

the SVR algorithm emerges as the optimal choice. This approach has strong generalization ability and can prevent the dimension disaster.

We evaluate several common regression prediction methods, including SVR, back propagation neural network (BPNN), and random forest (RF). The prediction error values are taken as a metric to assess the prediction performance across different methods. The results indicate that SVR is more suitable for the data used in this study compared to the other methods, providing more accurate prediction outcomes.

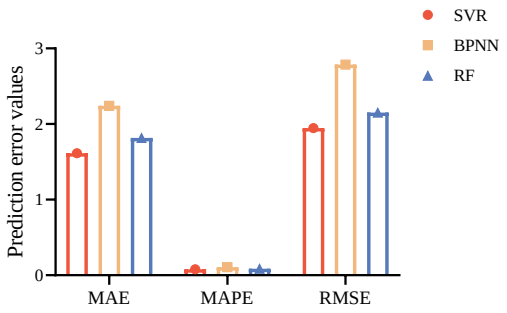

Figure 5. Prediction error values of different regression prediction methods.

4.3. Ablation study

We conduct an ablation study to validate CFSFSS in predicting cognitive function status in ESRD patients. Specifically, we evaluate the individual contributions of the functional subnetwork, mRMR feature selection, and E-WOA optimization algorithm by removing them separately. The aim is to assess their impact on prediction performance. As seen from Table 5, CFSFSS predicts cognitive functional status more accurately and with less error.

Table 5. Results of ablation experiments.

Functional subnetwork	mRMR feature selection	E-WOA optimization	MAE	MAPE	RMSE
×	√	√	1.2689	0.0574	1.9789
√	×	√	1.7230	0.0854	2.2547
√	√	×	1.5836	0.0771	1.9050
√	√	√	0.5951	0.0281	0.9994

4.4. Active brain regions

According to prediction results, the functional subnetwork extracted based on node betweenness centrality has the highest prediction accuracy. Node betweenness centrality is a measure of the importance of nodes in a network, which measures the degree to which a node acts as an intermediary or bridge in the network [37]. Therefore, eighteen brain regions with the highest node betweenness centrality in all ESRD group are identified, and the brain regions with strong activity are analyzed. Table 6 lists the active brain regions.

Table 6. Active brain regions.

Serial number	Brain regions	Abbreviations (L: Left, R: Right)	Color
66	Right angular gyrus	ANG.R	
14	Right triangular inferior frontal gyrus	IFGtriang.R	
38	Right hippocampus	HIP.R	
22	Right olfactory cortex	OLF.R	
46	Right cuneus	CUN.R	
17	Left rolandic operculum	ROL.L	
58	Right postcentral gyrus	PoCG.R	
16	Right orbital inferior frontal gyrus	ORBinf.R	
15	Left orbital inferiorfrontal gyrus	ORBinf.L	
72	Right caudate nucleus	CAU.R	
29	Left insula	INS.L	
24	Right medial superior frontal gyrus	SFGmed.R	
36	Right posterior cingulate gyrus	PCG.R	
2	Right precental gyrus	PreCG.R	
54	Right inferior occipital gyrus	IOG.R	
67	Left precuneus	PCUN.L	
60	Right superior parietal gyrus	SPG.R	
35	Left posterior cingulate gyrus	PCG.L	

The BrainNet Viewer toolbox [38] is adopted to visualize the active brain regions in the ESRD group and map them onto the ICBM152 template. Figure 6 shows the visualization results. As seen from the figure, most brain regions extracted according to the highest node betweenness centrality are distributed in the right side, including the right hippocampus (HIP.R), the right cuneus (CUN.R), the right posterior central gyrus (PoCG.R), the right posterior cingulate gyrus (PCG.R), and others. These brain regions play specific roles in different cognitive functions and neural processes, collectively contributing to cognition and functionality in the brain [39]. On the left hemisphere, there are brain regions such as the left insula (INS.L), left precuneus (PCUN.L), left postcentral gyrus (PCG.L), among others. They are involved in multiple cognitive and emotional processes, related to social cognition, spatial perception, attention, and working memory [40]. These brain regions are closely associated with the cognitive function status of the ESRD patients with cognitive impairment.

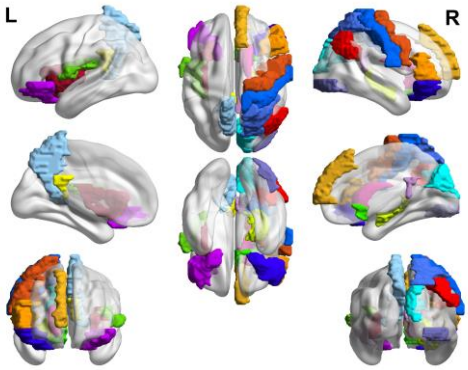

Figure 6. Distribution of active brain regions.

5. Discussion

We investigate the functional brain networks of ESRD patients accompanied by cognitive impairment. It explores the relationship between functional subnetwork scale determined by nodes from different network indicators and cognitive function status. A predictive model for MoCA scores is constructed by applying the AUC of the topological attribute parameters at the functional subnetwork scale. The features are carefully selected to enhance feature correlation learning and recognition through the E-WOA-optimized SVR, contributing to improve the performance in our study. The E-WOA-optimized SVR consistently yield lower prediction error values in Sub3 compared to the WOA-optimized SVR, achieving the optimal effect of prediction. These results highlight the enhanced performance of the E-WOA-optimized SVR in predicting clinical scores and demonstrate its potential for improved cognitive function assessment in ESRD patients.

The alterations in brain functional networks between the ESRD group and the NC group are uncovered through the analysis conducted by the functional subnetworks. It is discovered that the connectivity between brain regions have a complex and diverse impact on cognitive function status according to the topological attribute parameters at different functional subnetwork scales [41]. On one hand, connectivity can facilitate information transmission and coordination, thereby supporting the execution of different cognitive function. On the other hand, connectivity can also affect the regulation and manifestation of cognitive function such as attention, memory, and emotion [42]. In ESRD patients with cognitive impairment, the prefrontal lobe rete centrality index related to cognitive control is decreased, while the cingulate subnetwork centrality index related to emotional regulation shows a significant increase [43]. The results indicate that ESRD patients have notable abnormalities in cognitive control and emotional regulation, which may affect the psychological and behavioral status of patients [44].

It is worth mentioning that we find that patients have higher global efficiency and poorer local efficiency in the entire brain functional network. This indicates that the network's overall operation was more efficient. The information flow between local nodes in the ESRD group is relatively weaker than that in the NC group. These findings suggest that changes in the brain functional network of ESRD patients with cognitive impairment, which may be related to the disease course and pathophysiological mechanism of patients [45]. In the future, we will explore the mechanism of the influence of connections between different brain regions on cognitive function status, and propose more refined hypotheses and predictive models. It is possible to predict the cognitive function status of the patients with cognitive impairment more accurately by exploring the topological attribute parameters at functional subnetwork scale.

6. Conclusions

In summary, we proposed a method to predict the cognitive function status in the patients with ESRD at functional subnetwork scale (CFSFSS). The functional subnetworks formed by nodes based on different network indicators yield varying results in predicting cognitive function status. The prediction accuracy is improved by analyzing the functional subnetworks extracted from different network indicators and introducing the E-WOA to optimize the parameters of the SVR. The proposed method is validated on the existing dataset, with the MAE, MAPE, and RMSE of the prediction results amounting to 0.5951, 0.0281 and 0.9994, respectively. We further measure the node betweenness

centrality as an indicator of cognitive function status that has certain value in evaluating cognitive function status.

The proposed method involving functional subnetworks, network indicators, and the E-WOA optimization technique showcases promising results in predicting cognitive function status in patients with ESRD. Nevertheless, it is crucial to acknowledge the limitations of this study, such as the restricted number of samples in the dataset. Future research endeavors should focus on expanding the sample size and conducting multi-center studies to validate the broader applicability of the proposed method in a diverse patient population. Additionally, we use a cross-sectional study than a longitudinal study. Longitudinal studies with bigger samples should be conducted in the future to track cognitive function status and topological alterations at functional subnetwork scale, with the goal of gaining a deeper understanding of their relationship. Such efforts have the potential to offer valuable insights into cognitive impairment in ESRD patients and contribute to the optimization of treatment strategies.

Use of AI tools declaration

The authors declare that they have not used Artificial Intelligence (AI) tools in the creation of this article.

Acknowledgments

This work was supported by National Natural Science Foundation of China (grant No. 51877013), and Jiangsu Provincial Key Research and Development Program (grant No. BE2021636). This work was also sponsored by Qing Lan Project of Jiangsu Province.

Conflict of interest

The authors declare that there are no conflicts of interest.

References

1. *Centers for Disease Control and Prevention, Chronic kidney disease in the United States, 2019*, Atlanta, GA: US Department of Health and Human Services, Centers for Disease Control and Prevention, 2019. Available from: https://www.cdc.gov/kidneydisease/publications-resources/ckd-national-facts.html.
2. M. K. Tamura, K. Yaffe, Dementia and cognitive impairment in ESRD: diagnostic and therapeutic strategies, *Kidney Int*., **79** (2011), 14–22. https://doi.org/10.1038/ki.2010.336
3. L. A. Hawkins, S. Kilian, A. Firek, T. M. Kashner, C. J. Firek, H. Silvet, Cognitive impairment and medication adherence in outpatients with heart failure, *Heart Lung*, **41** (2012), 572–582. https://doi.org/10.1016/j.hrtlng.2012.06.001
4. M. K. Tamura, K. E. Covinsky, G. M. Chertow, K. Yaffe, C. S. Landefeld, C. E. McCulloch, Functional status of elderly adults before and after initiation of dialysis, *N. Engl. J. Med*., **361** (2009), 1539–1547. https://doi.org/10.1056/NEJMoa0904655
5. B. W. Zhou, X. Wang, Q. F. Yang, F. Q. Wu, L. Tang, J. Wang, et al., Topological alterations of the brain functional network in type 2 diabetes mellitus patients with and without mild cognitive impairment, *Front. Aging Neurosci.*, **14** (2022), 834319. https://doi.org/10.3389/fnagi.2022.834319

6. J. A. Contreras, J. Goñi, S. L. Risacher, E. Amico, K. Yoder, M. Dzemidzic, et al., Cognitive complaints in older adults at risk for Alzheimer's disease are associated with altered resting-state networks, *Alzheimer's Dementia: Diagn., Assess. Dis. Monit.*, **6** (2017), 40–49. https://doi.org/10.1016/j.dadm.2016.12.004
7. Z. Q. Jiao, Y. X. Ji, P. Gao, S. H. Wang, Extraction and analysis of brain functional statuses for early mild cognitive impairment using variational auto-encoder, *J. Ambient Intell. Hum. Comput.*, **14** (2020), 5439–5450. https://doi.org/10.1007/s12652-020-02031-w
8. X. L. Shen, E. S. Finn, D. Scheinost, M. D. Rosenberg, M. M. Chun, X. Papademetris, et al., Using connectome-based predictive modeling to predict individual behavior from brain connectivity, *Nat. Protoc.*, **12** (2017), 506–518. https://doi.org/10.1038/nprot.2016.178
9. X. Li, C. J. Yang, P. Xie, Y. Han, R. Su, Z. Y. Li, et al., The diagnosis of amnestic mild cognitive impairment by combining the characteristics of brain functional network and support vector machine classifier, *J. Neurosci Methods*, **363** (2021), 109334. https://doi.org/10.1016/j.jneumeth.2021.109334
10. B. Zhou, X. J. Dou, W. Wang, H. X. Yao, F. Feng, P. Wang, et al., Structural and functional connectivity abnormalities of the default mode network in patients with Alzheimer's disease and mild cognitive impairment within two independent datasets, *Methods*, **205** (2022), 29–38. https://doi.org/10.1016/j.ymeth.2022.06.001
11. D. Zhang, Y. Y. Chen, H. Wu, L. Lin, Q. Xie, C. Chen, et al., Associations of the disrupted functional brain network and cognitive function in end-stage renal disease patients on maintenance hemodialysis: A graph theory-based study of resting-state functional magnetic resonance imaging, *Front. Aging Neurosci.*, **15** (2021), 716719. https://doi.org/10.3389/fnhum.2021.716719
12. Y. Y. Zhang, Y. F. Xue, X. Wu, L. S. Qiao, Z. X. Wang, D. G. Shen, Selecting multiple node statistics jointly from functional connectivity networks for brain disorders identification, *Brain Topogr.*, **35** (2022), 559–571. https://doi.org/10.1007/s10548-022-00914-z
13. Y. Min, C. Liu, L. J. Zuo, Y. J. Wang, Z. X. Li, The relationship between altered degree centrality and cognitive function in mild subcortical stroke: A resting-state fMRI study, *Brain Res.*, **1798** (2023), 148125. https://doi.org/10.1016/j.brainres.2022.148125
14. J. H. Yu, M. M. Kanchi, I. Rawtaer, L. Feng, A. P. Kumar, E. H. Kua, et al., The functional and structural connectomes of telomere length and their association with cognition in mild cognitive impairment, *Cortex*, **132** (2020), 29–40. https://doi.org/10.1016/j.cortex.2020.08.006
15. Y. X. Mao, T. Q. Wang, M. L. Duan, H. Y. Men, Multi-objective optimization of semi-submersible platforms based on a support vector machine with grid search optimized mixed kernels surrogate model, *Ocean Eng.*, **260** (2022), 112077. https://doi.org/10.1016/j.oceaneng.2022.112077
16. W. Zeng, Y. K. Liao, Y. Chen, Q. Y. Diao, Z. Y. Fu, F. Y. Yao, Research on classification and recognition of the skin tumors by laser ultrasound using support vector machine based on particle swarm optimization, *Opt. Laser Technol.*, **158** (2023), 108810. https://doi.org/10.1016/j.optlastec.2022.108810
17. C. F. Ye, S. Mori, P. Chan, T. Ma, Connectome-wide network analysis of white matter connectivity in Alzheimer's disease, *NeuroImage: Clin.*, **22** (2019), 101690. https://doi.org/10.1016/j.nicl.2019.101690

18. S. H. Wang, Y. D. Zhang, G. Liu, P. Phillips, T. F. Yuan, Detection of Alzheimer's disease by three-dimensional displacement field estimation in structural magnetic resonance imaging, *J. Alzheimer's Dis.*, **50** (2016), 233–248. https://doi.org/10.3233/JAD-150848
19. Y. D. Zhang, Z. C. Dong, P. Phillips, S. H. Wang, G. Ji, J. Yang, et al., Detection of subjects and brain regions related to Alzheimer's disease using 3D MRI scans based on eigenbrain and machine learning, *Front. Comput. Neurosci.*, **9** (2015), 66. https://doi.org/10.3389/fncom.2015.00066
20. L. L. Sun, X. Y. Liang, D. N. Duan, J. Liu, Y. H. Chen, X. D. Wang, et al., Structural insight into the individual variability architecture of the functional brain connectome, *NeuroImage*, **259** (2022), 119387. https://doi.org/10.1016/j.neuroimage.2022.119387
21. S. Chakraborty, S. Sharma, A. K. Saha, S. Chakraborty, SHADE–WOA: A metaheuristic algorithm for global optimization, *Appl. Soft Comput.*, **113** (2021), 107866. https://doi.org/10.1016/j.asoc.2021.107866
22. M. Rubinov, O. Sporns, Complex network measures of brain connectivity: uses and interpretations, *NeuroImage*, **52** (2010), 1059–1069. https://doi.org/10.1016/j.neuroimage.2009.10.003
23. M. P. van den Heuvel, R. C. Mandl, C. J. Stam, R. S. Kahn, H. E. Hulshoff Pol, Aberrant frontal and temporal complex network structure in schizophrenia: a graph theoretical analysis, *J. Neurosci.*, **30** (2010), 15915–15926. https://doi.org/10.1523/JNEUROSCI.2874-10.2010
24. F. Özyurt, A fused CNN model for WBC detection with MRMR feature selection and extreme learning machine, *Soft Comput.*, **24** (2020), 8163–8172. https://doi.org/10.1007/s00500-019-04383-8
25. X. Y. Liang, C. H. Yeh, A. Connelly, F. Calamante, A novel method for extracting hierarchical functional subnetworks based on a multisubject spectral clustering approach, *Brain connect.*, **9** (2019), 399–414. https://doi.org/10.1089/brain.2019.0668
26. D. Zhang, Y. Y. Chen, H. Wu, L. Lin, Q. Xie, C. Chen, et al., Associations of the Disrupted Functional Brain Network and Cognitive Function in End-Stage Renal Disease Patients on Maintenance Hemodialysis: A Graph Theory-Based Study of Resting-State Functional Magnetic Resonance Imaging, *Front. Hum. Neurosci.*, **15** (2021), 716719. https://doi.org/10.3389/fnhum.2021.716719
27. M. H. Nadimi-Shahraki, H. Zamani, S. Mirjalili, Enhanced whale optimization algorithm for medical feature selection: A COVID-19 case study, *Comput. Biol. Med.*, **148** (2022), 105858. https://doi.org/10.1016/j.compbiomed.2022.105858
28. W. H. He, J. J. Wang, Y. P. Liu, Z. P. Qin, C. M. Sun, H. You, et al., A Novel Symmetrical Peak Fitting Method Based on Improved WOA Algorithm for the Analysis of Microchip Electrophoresis Signals, *Symmetry*, **14** (2022), 2603. https://doi.org/10.3390/sym14122603
29. J. Du, H. Zhu, J. Zhou, P. W. Lu, Y. G. Qiu, L. Yu, et al., Structural brain network disruption at preclinical stage of cognitive impairment due to cerebral small vessel disease, *Neuroscience*, **449** (2020), 99–115. https://doi.org/10.1016/j.neuroscience.2020.08.037
30. F. Fang, Y. Gao, P. E. Schulz, S. Selvaraj, Y. Zhang, Brain controllability distinctiveness between depression and cognitive impairment, *J. Affective Disord.*, **294** (2021), 847–856. https://doi.org/10.1016/j.jad.2021.07.106
31. I. Lazarou, S. Nikolopoulos, S. I. Dimitriadis, I. Y. Kompatsiaris, M. Spilioti, M. Tsolaki, Is brain connectome research the future frontier for subjective cognitive decline? A systematic review, *Clin. Neurophysiol.*, **130** (2019), 1762–1780. https://doi.org/10.1016/j.clinph.2019.07.004

32. X. B. Chen, H. Zhang, Y. Gao, C. Y. Wee, G. Li, D. G. Shen, High-order resting-state functional connectivity network for MCI classification, *Hum. Brain Mapp.*, **37** (2016), 3282–3296. https://doi.org/10.1002/hbm.23240
33. C. D. Yang, P. Y. Wang, J. Tan, Q. S. Liu, X. W. Li, Autism spectrum disorder diagnosis using graph attention network based on spatial-constrained sparse functional brain networks, *Comput. Biol. Med.*, **139** (2021), 104963. https://doi.org/10.1016/j.compbiomed.2021.104963
34. J. H. Wang, X. D. Wang, M. R. Xia, X. H. Liao, A. Evans, Y. He, GRETNA: a graph theoretical network analysis toolbox for imaging connectomics, *Front. Hum. Neurosci.*, **9** (2015), 386. https://doi.org/10.3389/fnhum.2015.00386
35. F. Belotti, F. Peracchi, Fast leave-one-out methods for inference, model selection, and diagnostic checking, *Stata J.*, **20** (2020), 785–804. https://doi.org/10.1177/1536867X20976312
36. J. J. Zhu, Y. F. Qian, B. Zhang, X. H. Li, Y. Bai, X. S. Li, et al., Abnormal synchronization of functional and structural networks in schizophrenia, *Brain Imaging Behav.*, **14** (2020), 2232–2241. https://doi.org/10.1007/s11682-019-00175-8
37. Y. D. Zhang, S. H. Wang, P. Phillips, J. Q. Yang, T. F. Yuan, Three-dimensional eigenbrain for the detection of subjects and brain regions related with Alzheimer's disease, *J. Alzheimer's Dis.*, **50** (2016), 1163–1179. https://doi.org/10.3233/JAD-150988
38. M. R. Xia, J. H. Wang, Y. He, BrainNet Viewer: a network visualization tool for human brain connectomics, *PloS one*, **8** (2013), e68910. https://doi.org/10.1371/journal.pone.0068910
39. Y. Liang, Y. J. Chen, H. Li, T. D. Zhao, X. Sun, N. Shu, et al., Disrupted functional connectivity related to differential degeneration of the cingulum bundle in mild cognitive impairment patients, *Curr. Alzheimer Res.*, **12** (2015), 255–265. https://doi.org/10.2174/1567205012666150302155336
40. Y. D. Zhang, S. H. Wang, Y. X. Sui, M. Yang, B. Liu, H. Cheng, et al., Multivariate approach for Alzheimer's disease detection using stationary wavelet entropy and predator-prey particle swarm optimization, *J. Alzheimer's Dis.*, **65** (2018), 855–869. https://doi.org/10.3233/JAD-170069
41. B. Zhou, X. J. Dou, W. Wang, H. X. Yao, F. Feng, P. Wang, et al., Structural and functional connectivity abnormalities of the default mode network in patients with Alzheimer's disease and mild cognitive impairment within two independent datasets, *Methods*, **205** (2022), 29–38. https://doi.org/10.1016/j.ymeth.2022.06.001
42. A. F. Struck, M. Boly, G. Hwang, V. Nair, J. Mathis, A. Nencka, et al., Regional and global resting-state functional MR connectivity in temporal lobe epilepsy: Results from the Epilepsy Connectome Project, *Epilepsy Behav.*, **117** (2021), 107841. https://doi.org/10.1016/j.yebeh.2021.107841
43. Y. Min, C. Liu, L. J. Zuo, Y. J. Wang, Z. X. Li, The relationship between altered degree centrality and cognitive function in mild subcortical stroke: A resting-state fMRI study, *Brain Res.*, **1798** (2023), 148125. https://doi.org/10.1016/j.brainres.2022.148125
44. Z. Q. Jiao, T. X. Jiao, J. H. Zhang, H. F. Shi, B. N. Wu, Y. D. Zhang, Sparse structure deep network embedding for transforming brain functional network in early mild cognitive impairment classification, *Int. J. Imaging Syst. Technol.*, **31** (2021), 1197–1210. https://doi.org/10.1002/ima.22531

45. C. S. Tang, M. Y. Wei, J. D. Sun, S. H. Wang, Y. D. Zhang, CsAGP: Detecting Alzheimer's Disease from Multimodal Images via Dual-Transformer with Cross-Attention and Graph Pooling, *J. King Saud Univ. Comput. Inf. Sci.*, **35** (2023), 101618. https://doi.org/10.1016/j.jksuci.2023.101618